



HAL
open science

Timing of thermal metamorphism in CM chondrites: Implications for Ryugu and Bennu future sample return

Elsa Amsellem, Frédéric Moynier, Brandon Mahan, Pierre Beck

► To cite this version:

Elsa Amsellem, Frédéric Moynier, Brandon Mahan, Pierre Beck. Timing of thermal metamorphism in CM chondrites: Implications for Ryugu and Bennu future sample return. *Icarus*, 2020, 339, pp.113593. 10.1016/j.icarus.2019.113593 . insu-02916325

HAL Id: insu-02916325

<https://insu.hal.science/insu-02916325>

Submitted on 7 Mar 2022

HAL is a multi-disciplinary open access archive for the deposit and dissemination of scientific research documents, whether they are published or not. The documents may come from teaching and research institutions in France or abroad, or from public or private research centers.

L'archive ouverte pluridisciplinaire **HAL**, est destinée au dépôt et à la diffusion de documents scientifiques de niveau recherche, publiés ou non, émanant des établissements d'enseignement et de recherche français ou étrangers, des laboratoires publics ou privés.



Distributed under a Creative Commons Attribution - NonCommercial 4.0 International License

38 in Antarctica, Yamato 793321 and Belgica 7904, because of the presence of an “intermediate
39 phase” with “transformed” phyllosilicates, indicating matrix heating at a later stage than
40 aqueous alteration (Akai, 1988). The matrix of typical CM chondrites is composed largely of
41 the hydrous minerals serpentine (Mg-Fe silicate) and tochilinite (Fe sulphide), however most
42 of the heated CM meteorites contain Fe-rich olivine, low Ca pyroxene and troilite (Fe
43 sulphide) consistent with dehydration of the matrix minerals (Nakamura, 2005).

44 Heated meteorites show depletion in water content (Garenne et al., 2014), C (relative
45 to H) (Alexander et al., 2013), trapped noble gases (Nakamura et al., 2006) and in highly and
46 moderately volatile or labile elements (Rb, Cs, Se, Ag, Te, Zn, In, Bi, Tl; e.g., Wang and
47 Lipschutz, 1998). The heating origin for these features is confirmed by the absence or lower
48 amount of phyllosilicates and their dehydrated matrix compared to typical CM chondrites
49 (e.g. Nakato et al., 2013), as well as higher organic maturity (Quirico et al., 2013, 2018).

50 Evaporation has been demonstrated as the origin for volatile element loss in these
51 meteorites through stable isotopic measurements of Zn and Rb (Mahan et al. 2018, Pringle
52 and Moynier 2017). Mahan et al. (2018) analysed different heated CMs for Zn isotopic
53 composition and found that they are enriched in the heavier isotopes of Zn, most notably for
54 PCA 02010 and PCA 02012, suggesting evaporation in an open system as the main culprit for
55 Zn (and other volatile element) loss. Similarly, Pringle and Moynier (2017) reported high
56 $^{87}\text{Rb}/^{85}\text{Rb}$ ratios associated with low Rb concentration for the same CMs, implying volatile
57 loss during evaporation consistent with Rb fractionation under partial isotope equilibration
58 between the evaporated gas and the residue. Cumulatively, these results lead to only three
59 possible heating sources, either during the first Myrs of the solar system via short-lived
60 radioactive heating, or later by impact induced heating or solar radiation when approaching
61 the Sun. Presently, the main argument in favour of short duration heating, i.e. not from
62 radioactive decay, is based on the absence of Fe-Mg diffusion into chondrules of the heated
63 CM PCA 02012, as longer heating would lead to diffusion patterns (Nakato et al., 2013),
64 however this argument does not remark on the actual dates of events. Determining the timing
65 of the heating events can bring resolution to this longstanding issue.

66 Here, we report Rb-Sr model ages of 5 heated CM chondrites (PCA 02012, PCA
67 02010, PCA 91008, QUE 93005 and MIL 07675). The ^{87}Rb - ^{87}Sr radioactive decay system
68 ($\lambda^{87}\text{Rb} = 1.393 \times 10^{-11} \text{ yr}^{-1}$; Nebel et al. 2011) is well suited to date volatile depletion events
69 (e.g Papanastassiou and Wasserburg, 1969; Moynier et al., 2012; Hans et al., 2013). This is
70 because Rb is relatively volatile (50% condensation temperature, T_{CRb} , of 800 K, Lodders
71 2003) while Sr is relatively refractory ($T_{\text{CSr}} = 1404 \text{ K}$) implying a chemical fractionation of Rb
72 and Sr during a volatilisation process. Heated CM chondrites have lost up to 90% of their Rb
73 during thermal metamorphism leading to extremely low Rb/Sr ratios. If we assume a single
74 stage fractionation model in which the Rb/Sr is fractionated from an unheated CM (for

75 example equivalent to the CM chondrite Murchison), a model age of the volatilization event
76 can be estimated from the $^{87}\text{Sr}/^{86}\text{Sr}$ ratio and the Rb/Sr ratio of the heated CM (Figure 1).
77 Figure 1 presents the different evolution trends of the $^{87}\text{Sr}/^{86}\text{Sr}$ for a non-heated chondrite
78 (trend without perturbation) and heated chondrites (the evolution is changed after the heating
79 event, where a part of Rb is lost from the system). We find that the ages of Rb/Sr
80 fractionation are relatively recent (<2 Ga), implying that the CM were heated after the
81 formation of their parent bodies and therefore not due to ^{26}Al radioactive decay. A possible
82 heat source at this later stage could be represented by impacts. Collisions between asteroids
83 are thought to generate asteroid families. We therefore compare the epoch of meteorite
84 heating events with the ages of some known asteroid collisional families, involving asteroids
85 belonging to the spectroscopic C-types, which have been associated to carbonaceous
86 chondrites.

87

88

89 2) Material and method

90

91 This section presents briefly the meteorite samples including their heating
92 characteristics and presents the method used to estimate the timing of the heating events. This
93 method leans on the Rb to Sr radioactive decay. During a heating event, the more volatile
94 elements (e.g., Rb) are preferentially lost from the system compared to more refractory
95 elements (e.g., Sr). This leads to a fractionation between Rb and Sr. The loss of Rb in the
96 asteroid parent body would change the evolution of the production of the radiogenic ^{87}Sr
97 (represented by the $^{87}\text{Sr}/^{86}\text{Sr}$ ratio). Comparing the heated chondrites with non-heated
98 chondrites enables us to estimate the timing of this fractionation, corresponding to the heating
99 event.

100

101 2.1) Samples and descriptions

102 A set of USGC standards were analysed as method validation: BIR-1a (Icelandic
103 basalt); STM-2 (Table Mountain Syenite); AGV-2 (Guano Valley Andesite) and BCR-2
104 (Columbia River Basalt). For the CM chondrites, five Antarctic samples (PCA 02012, PCA
105 02010, PCA 91008, QUE 93005 and MIL 07675) were chosen to represent a variety of
106 thermally metamorphosed CMs. They are all considered as heated chondrites but the degree
107 of heating varies between them.

108 PCA 02012 was first recognised as a thermally metamorphosed CM in the study of
109 Nakato et al. (2013). The matrix is dehydrated and presents a high organic maturity but the
110 elemental composition is close to typical CM2 chondrites. They estimate the temperature of
111 the heating event to be approximately 900°C, as this meteorite compared with experimentally

112 heated CM chondrites from the study of Nakato et al. (2008) share similar features. PCA
113 02012 represents a stage IV (strongly heated) according to the heating stage classification of
114 Nakamura et al. (2005).

115 Stable isotopic compositions of PCA 02012 and PCA 02010 have been performed for
116 Rb, Zn, H, (C and N) isotopes (Alexander et al., 2013; Mahan et al., 2018; Pringle and
117 Moynier, 2017), with Rb and Zn in particular suggesting heating and volatile loss in an open
118 system. These two chondrites have lost between 40% and 90% of Rb during one or several
119 events (Pringle and Moynier, 2017) confirming the temperature of the heating source
120 estimated, since the half condensation temperature of Rb is $T_c = 800\text{K}$ (Lodders et al., 2003).

121 PCA 91008 shows depletion in most thermally mobile trace elements suggesting loss
122 during heating (Wang and Lipschutz, 1998) and was classified as heating stage III containing
123 a poorly crystalline dehydrated phyllosilicate phase in the matrix (Nakamura et al., 2005).
124 PCA 91008 shows evidence of terrestrial weathering by the analysis of the matrix and
125 chondrules mineralogy and their textures (Tonui et al., 2014). Conventional stable isotopic
126 compositions (δD , $\delta^{18}\text{O}$, $\delta^{13}\text{C}$ and $\delta^{15}\text{N}$) were obtained by Alexander et al. (2010, 2013).
127 Transmission infrared spectra were obtained on PCA 02010 and PCA 91008 to reveal
128 dehydration trends with phyllosilicates replaced by olivine (Beck et al., 2014), confirming
129 earlier results of Tonui et al. (2002) and Quirico et al. (2011).

130 Loss of hydrogen is estimated for the three PCA meteorites suggesting a dehydration
131 event (Garenne et al., 2014). Furthermore, the content of C and H of the three meteorites
132 relative to the isotopic composition of H reveals a severe heating process to explain the loss
133 of C preferentially relative to H (Alexander et al., 2013).

134 QUE 93005 was studied for petrological observations, aqueous alteration processes
135 and O isotopic composition and was not viewed as thermally metamorphosed in these studies
136 especially because it contain hydrated minerals (Rubin et al., 2012; Rubin et al., 2007;
137 Clayton and Mayeda, 1999), however, it was classified as a heated CM (Alexander et al.
138 2012, 2013) because of its low hydrogen abundance correlating with H isotopic composition
139 similar with other heated CMs including MIL 07675 and PCA 91008. In addition, Raman
140 spectra of QUE 93005 are similar to the three PCA meteorites studied here (Quirico et al.,
141 2013). The analysis of insoluble organic matter's composition and structure shows evidence
142 for a thermal event but the presence of hydrated minerals argues against a thermal process.
143 Quirico et al. (2018) have suggested that QUE 93005 experienced retrograde aqueous
144 alteration, following the thermal event, which erased dehydration signatures.

145 The five chondrites contain carbonates that were analysed by Alexander et al. (2015)
146 for C and O isotopic composition. The three PCA samples and MIL 07675 show the lowest

147 carbonate content and the lowest $\delta^{13}\text{C}$ in carbonate compared to other CMs revealing a
148 heating event.

149

150 2.2) Sample preparation

151 Rb-Sr chronology method requires the precise calculation of concentrations of Rb and
152 Sr in the bulk samples to obtain the $^{87}\text{Rb}/^{86}\text{Sr}$ ratio and the determination of the $^{87}\text{Sr}/^{86}\text{Sr}$ ratio.
153 The concentration of Rb and Sr is determined by isotope dilution technique that is based on
154 adding a tracer enriched in a single isotope (^{84}Sr and ^{87}Rb) to an aliquot of the samples and
155 then determining the concentration via isotopic measurement. The optimum amount of spike
156 added is determined by minimizing the error propagation on the calculated sample
157 concentration. Previously calibrated spikes were added as solutions to the powdered sample
158 prior to digestion in order to let spike and sample equilibrate, and spiked and un-spiked
159 samples were digested in two steps. The powders were dissolved in a 3:1 mixture of
160 concentrated HF and concentrated HNO_3 and placed on a hot plate for 2 days at 120°C . The
161 samples were evaporated to dryness and concentrated hydrochloric acid was added during 1
162 day at 120°C . The $^{87}\text{Sr}/^{86}\text{Sr}$ ratio was determined on the unspiked samples following
163 purification by ion exchange chromatography using 200 μL of pre-cleaned Sr-specific resin
164 (Eichrom, 20-50 μm), following a protocol previously described (Amsellem et al., 2018).
165 Briefly, the spiked samples were purified in order to elute both Rb and Sr. Rubidium was first
166 purified on a pre-cleaned AG50X12 cation exchanged resin following one step of purification
167 scheme following Pringle and Moynier (2017). The 1.8mL resin was conditioned with 3N
168 HCl and the sample was loaded in 3N HCl. The matrix was eluted in 4mL of 3N HCl and the
169 Rb was eluted with 6mL of 3N HCl. The matrix was collected to separate Sr from the other
170 elements using the Sr-specific resin afterwards. The resin was conditioned with 3N HNO_3 and
171 the sample was loaded in 3N HNO_3 , Sr was eluted with Milli-Q H_2O water after the elution of
172 the matrix with 3N HNO_3 . Two different powders ($m_1= 114.3$ mg and $m_2= 95.5$ mg) of PCA
173 02012 were made through the entire chemistry process from the digestion to the
174 measurement.

175

176 2.3) Measurements

177

178 Measurements of the Sr (both for natural isotopic composition and isotope dilution)
179 and Rb (for isotope dilution) isotopic composition of the samples were performed in medium
180 resolution mode on a Thermo Fisher Neptune Plus MC-ICP-MS located at the Institut de
181 Physique du Globe de Paris (IPGP), during three different sessions. Samples were introduced
182 using a cyclonic spray chamber. The intensities of ^{82}Kr , ^{83}Kr , ^{84}Sr , ^{85}Rb , ^{86}Sr , ^{87}Sr and ^{88}Sr

183 were collected using Faraday cups. We performed on-peak-zeros prior to each sequence and
184 frequently during the sequence to monitor Kr interferences on mass ^{84}Sr and ^{86}Sr .

185 For the Sr natural isotopic measurement, the mass-dependent fractionations (natural
186 and instrumental), on the $^{87}\text{Sr}/^{86}\text{Sr}$ ratio were corrected through internal normalization to a
187 $^{86}\text{Sr}/^{88}\text{Sr}$ value of 0.1194. The accuracy of the $^{87}\text{Sr}/^{86}\text{Sr}$ ratio were confirmed by analysing the
188 NIST SRM987 standard giving a value of 0.71029 ± 0.00004 which falls in between the
189 certificate value (0.71034) and the commonly accepted value (0.71026) (Balcaen et al., 2005).
190 For the isotope dilution measurements of Sr and Rb, the $^{84}\text{Sr}/^{86}\text{Sr}$ ratio and $^{87}\text{Rb}/^{85}\text{Rb}$ ratio
191 were measured respectively.

192

193

194 3) Results

195 The $^{87}\text{Sr}/^{86}\text{Sr}$ and $^{87}\text{Rb}/^{86}\text{Sr}$ ratios are presented in Table 1 for the standard rocks and
196 the five bulk chondrites. The Rb and Sr concentration of the standards are compared with the
197 literature data (USGS Certificate of Analysis and published values) in Figure 2a and 2b. The
198 Sr concentration are similar with the literature within error except for STM-2 where there is
199 10% of difference with USGS data but is within error compared to Schudel et al. (2015). The
200 Rb concentrations are similar within error compare to the literature. The $^{87}\text{Sr}/^{86}\text{Sr}$ of the
201 standards are compared with the literature in Figure 2c. The Rb concentration of BIR-1a is
202 not presented, as an incorrect amount of spiked solution was added in the sample leading to
203 an incorrect value.

204 Rubidium concentrations of the five heated chondrites are all lower than typical CM
205 (Murchison; ~ 1.6 ppm; Mittlefehldt and Wetherill, 1979 and Pringle and Moynier 2017,
206 Figure 3), and for PCA 02010 (Rb= 0.24ppm) it is consistent with concentrations obtained
207 previously during isotopic measurements after intensive Rb chemical purification and by
208 comparing the intensity of the Rb of the sample with a standard of known concentration (Rb=
209 0.2ppm, Pringle and Moynier, 2017). PCA 02010 and PCA 02012 chondrites show similar Sr
210 concentration with typical CM (Murchison; ~ 10 ppm; Mittlefehldt and Wetherill, 1979)
211 whereas PCA 91008, QUE 93005 and MIL07675 are depleted in Sr compared to typical CM.
212 QUE 93005 is depleted in Rb, which could be related to evaporation of Rb without affecting
213 the hydrated minerals. The $^{87}\text{Sr}/^{86}\text{Sr}$ ratio of the heated chondrites (from 0.72438 ± 0.00009 to
214 0.73010 ± 0.00014) are within the range but slightly lower of typical CM chondrites (from
215 0.72765 ± 0.00005 to 0.73240 ± 0.00095 ; Mittlefehldt and Wetherill, 1979). The $^{87}\text{Rb}/^{86}\text{Sr}$
216 range from 0.043 ± 0.001 to 0.326 ± 0.003 and are lower compared to the non-heated CM
217 chondrites (~ 0.4 ; Mittlefehldt and Wetherill, 1979). The two different powders of PCA 02012

218 show slight differences in Rb concentration and in $^{87}\text{Sr}/^{86}\text{Sr}$ ratio reflecting the heterogeneity
 219 of the sample.

220 The chondrites from this study are Antarctic finds and are thus subjected to terrestrial
 221 alteration. However, the effect of alteration on Sr would not affect the results as we internally
 222 normalize the isotope ratios to $^{86}\text{Sr}/^{88}\text{Sr}$, correcting for mass dependent fractionations such as
 223 the ones due to alteration processes. Furthermore, there is no clear correlation between Rb
 224 and weathering grades (data from Alexander et al., 2012) and Rb abundances in Antarctic CM
 225 chondrites and non-Antarctic ones are similar, suggesting that Rb is not affected by alteration
 226 for these samples. The Rb loss of the meteorites studied does not seem to correlate with their
 227 heating stages (Tables 1 and 2). This is at odds with the isotopically fractionated Rb of two of
 228 them that points toward volatile loss by evaporation. The absence of correlation might rather
 229 reflect the occurrence of different parameters in the loss of Rb, such as duration of the heating
 230 or efficiency of the Rb loss. The heating stage is based on the matrix mineralogy and then
 231 does not take into account others parameters.

232

233

234 4) Discussion

235 The timing of the Rb/Sr fractionation can be estimated using a 2-stage model in
 236 which the first stage is the evolution of a CM chondrite reservoir formed at T_0 (4.567 Ga,
 237 Connelly et al., 2012) and the second stage represents the Rb/Sr fractionation event that
 238 occurred at time T_H using the following equations, where T corresponds to the present time
 239 and λ the decay constant rate:

240

241

$$242 \quad \left(\frac{^{87}\text{Sr}}{^{86}\text{Sr}}\right)_T = \left(\frac{^{87}\text{Sr}}{^{86}\text{Sr}}\right)_{T_H} + \left(\frac{^{87}\text{Rb}}{^{86}\text{Sr}}\right)_{T_H} \times (e^{\lambda(T-T_H)} - 1) \quad \text{Eq.1}$$

243

$$244 \quad \left(\frac{^{87}\text{Sr}}{^{86}\text{Sr}}\right)_H = \left(\frac{^{87}\text{Sr}}{^{86}\text{Sr}}\right)_{NH} = \left(\frac{^{87}\text{Sr}}{^{86}\text{Sr}}\right)_{NH} + \left(\frac{^{87}\text{Rb}}{^{86}\text{Sr}}\right)_{NH} \times (e^{\lambda(T_H-T_0)} - 1) \quad \text{Eq.2}$$

245

246

$$247 \quad T_H = -\frac{1}{\lambda} \ln\left(\frac{\left(\frac{^{87}\text{Sr}}{^{86}\text{Sr}}\right)_T - \left(\frac{^{87}\text{Sr}}{^{86}\text{Sr}}\right)_{NH}}{\left(\frac{^{87}\text{Rb}}{^{86}\text{Sr}}\right)_T - \left(\frac{^{87}\text{Rb}}{^{86}\text{Sr}}\right)_{NH}}\right) \quad \text{Eq.3}$$

248

249

250

251

252 Equation 1 represents the radioactive decay equation showing the production of the
253 radiogenic ^{87}Sr over the stable ^{86}Sr of a heated chondrite from the present time T to T_H (timing
254 of the heating event). Equation 2 represents the evolution of the $^{87}\text{Sr}/^{86}\text{Sr}$ for a non-heated
255 chondrite and heated chondrite (which is the same) from T_0 to T_H . Here, the assumption is
256 that the initial $^{87}\text{Sr}/^{86}\text{Sr}$ and $^{87}\text{Rb}/^{86}\text{Sr}$ ratios of the heated chondrites (subscript H) were similar
257 to the ones of the non-heated chondrites (subscript NH). The timing of the heating event
258 (Equation 3) is deduced by Equations 1 and 2.

259

260 The $^{87}\text{Sr}/^{86}\text{Sr}$ and $^{87}\text{Rb}/^{86}\text{Sr}$ ratios of non-heated chondrites is slightly variable (Mittlefehldt
261 and Wetherill, 1979; Kaushal and Wetherill, 1970) and therefore introduce an uncertainty in
262 the estimation of the heating age as the calculated timing will depend on which non-heated
263 CM is chosen as reference. Here, we decided to use the two non-heated CMs that represent
264 the most primitive chondrites in terms of heating event (Quirico et al., 2018) and with the
265 most extreme $^{87}\text{Rb}/^{86}\text{Sr}$ and $^{87}\text{Sr}/^{86}\text{Sr}$ ratio (Mighei and Murchison, Mittlefehldt and Wetherill,
266 1979; Kaushal and Wetherill, 1970) in order to obtain the most conservative errors. This
267 calculation has been done for each of the 5 heated CM chondrites and the results are
268 presented in Table 2 and Figure 4. The ages range between $1.54 \text{ Ga} \pm 0.48 \text{ Ga}$ and 607 ± 614
269 Ma ago, indicating that all heating events herein were younger than 2.02Ga.

270 This represents the first dating of the thermal metamorphism of CM chondrites and
271 indicates that these events occurred relatively late in Solar System history. This observation
272 excludes radioactive decay of ^{26}Al as the source of heating for CM metamorphism as it would
273 have all decayed away a long time before (~less than 10Myrs after Solar System formation,
274 e.g., Lee et al., 1977). This result alone provides a major step in our understanding of the
275 mechanisms of heating for metamorphism.

276 The two alternative sources of heating that could occur later in the Solar System
277 history are solar heating and heat released during impacts. Solar radiation on asteroids could
278 occur when a body approaches the Sun. The two recent CM chondrite falls Sutters's Mill and
279 Maribo both had perihelion distances below 0.5 A.U. (Jenniskens et al., 2012). This implies
280 an equilibrium temperature around 550 K at the subsolar point (at perihelion, using an albedo
281 of 0.01), which is a minima since the orbital evolution prior to delivery on Earth may have
282 encompassed even closer approaches to the Sun (Marchi et al., 2009). If the heating is due to
283 solar radiation, one will expect young ages for the heating event, of the order of the Cosmic-
284 Ray Exposure (CRE) age obtained on carbonaceous chondrites (typically $< 2 \text{ Myrs}$, Eugster et
285 al., 2006). The age determined for PCA 91008 is much older than these CRE ages as well as
286 typical transfer that can be estimated from solar system dynamics (Morbidelli and Gladman,
287 1998). In the case of the 4 other samples, the error on the ages does not allow us to strictly
288 rule out solar radiation.

289 Our data cannot settle this issue but petrographic studies of PCA 02012 suggest that
290 the heating event may have lasted less than 10 seconds and at ~900°C (Nakato et al., 2013).
291 This is based on the Fe-Mg interdiffusion between chondrules, the thermal maturation of the
292 organic matter, and the texture of the matrix. This short duration is in agreement with the
293 expected duration of impact metamorphism (Beck et al., 2005).

294 In addition, QUE 93005 seems not to have been homogeneously heated. It has kept
295 some hydrated minerals while lost >50% of its Rb. The heterogeneous temperature
296 distribution may be representative of impact heating, as depending on the porosity of the
297 sample, a higher post-shock temperature is induced and may be heterogeneously distributed
298 (Schmitt et al., 1994). This sample is the least heated chondrite from this study and has also a
299 very weak evidence of shock (shock stage S1, Rubin et al., 2012). All together, the late ages,
300 the petrographic features and the heterogeneous heating suggests that impact heating is the
301 most likely source of heating to explain the thermal metamorphism of CM chondrites. C-type
302 asteroids are the most common asteroids in the main belt and are the closest spectral
303 analogues to carbonaceous chondrites (e.g., Johnson and Fanale, 1973; Chapman et al., 1975).
304 We will now discuss the relationship between the impacts at the origin of the thermal
305 metamorphism observed in the chondrites and the collisional history of C-type asteroids.

306 Shock experiments conducted on Murchison have showed that in order to dehydrate
307 phyllosilicates and form Fe-sulfide, olivine and pyroxene, an impact pressure of at least 30
308 GPa is needed (Tomeoka et al., 2003). This corresponds to a velocity impact of ~2 km.s⁻¹ for
309 a metallic impactor (Tyburczy et al., 1986), for a silicate one the velocity is expected to be
310 higher which would be close to the mean value of 5 km.s⁻¹ in the asteroid belt (Farinella and
311 Davis, 1992). Therefore, physical conditions required to heat the CM chondrites are on par
312 with those encountered in the asteroid main-belt (e.g., Wasson et al., 1987; Rubin, 1995).
313 Furthermore, the similarity in the reflectance spectra between naturally heated CMs,
314 experimentally heated CMs and some type-C, G, B and F asteroids have already suggestively
315 been linked with the same process: impacts in the asteroid belt (Hiroi et al., 1993). This is
316 consistent with the recent results of reflectance spectra on Ryugu's surface from the
317 Hayabusa2 mission that are similar to thermally or shock-metamorphosed carbonaceous
318 chondrites (Kitazato et al., 2019; Sugita et al., 2019). However, metamorphosed CI and CM
319 chondrites have been suggested not to represent the surface material of asteroids B, C, Cb and
320 Cg (BCG) types as the density expected for heated asteroids would be higher than those of Ch
321 and Cgh types (hydrated type asteroids) which is not the case for BCG types asteroids
322 (Vernazza et al., 2015). Thus, the association of heated chondrites with their asteroid
323 counterparts is not clear.

324 There are three types of collision that might have played a role in setting the age of
325 heated CM chondrites. The Rb loss might have occurred during different heating events. CMs

326 are thought to have been compacted by a series of impact events (Lindgren et al., 2015),
327 which would lead to different heating events. Our age would then represent a minimum age
328 for these events.

329

330 i) First, we can think of “old collisions”, related to the initial accretion phases of the
331 Solar System. In that case, we would expect the heating ages to be similar to the K/Ar ages of
332 lunar samples, typically 3.8 Gyrs and older. This is not the case for the heated CM chondrites
333 measured here. This excludes direct ejection of the meteorites from a large primordial C-type
334 with an old and heavily cratered surface.

335 ii) Second, collisions in the asteroid belt are still occurring and the asteroid family
336 represents the main source of meteorites (Vernazza, 2008; 2014) hence the young ages of the
337 heating event of the CM chondrites could be due to collisions forming asteroid families.
338 Collision ages of C-type asteroid families can be compared to the ages obtained here for CM
339 chondrites to discern whether the collisional heating could be related to disruptive, family
340 forming, impacts (Figure 4). The ages of the collisions that created different asteroids families
341 are estimated by modelling the spreads of the orbital parameter of family members due to the
342 Yarkovsky effect (Brož et al., 2013; Bottke et al., 2015; Spoto et al., 2015; Milani et al., 2014,
343 2017; Paolicchi et al., 2018). Asteroid family Misa, Erigone, Naema, Astrid, Brasilia and
344 1993 FY12 (C-types, Carruba et al., 2013) have ages (259 ± 95 Ma, 224 ± 36 Ma, 206 ± 45
345 Ma, 156 ± 23 Ma, 150 ± 23 Ma, 143 ± 56 Ma and 83 ± 21 Ma; Paolicchi et al., 2018) similar
346 within error to the heating ages estimated here for PCA 02012, PCA 02010, MIL 07675 and
347 QUE 93005. Prokne, Hygiea, Euphrosyne, Klumpkea, Dora, Hoffmeister, Astrae (C-types,
348 Carruba et al., 2013), New Polana and Eulalia (Walsh et al., 2013) asteroid family with ages
349 of (1448 ± 348 Ma, 1347 ± 220 Ma, 1225 ± 304 Ma, 663 ± 154 Ma, 506 ± 116 Ma, 463 ± 110
350 Ma, 332 ± 67 Ma, 329 ± 50 Ma, 328 ± 71 Ma, 1.4 ± 0.15 Ga and 0.8 ± 0.1 Ga respectively;
351 Paolicchi et al., 2018 and Bottke et al., 2015) are similar to PCA 91008, PCA 02012 and QUE
352 93005 (Figure 4). The two asteroids Prokne and Euphyrosyne have surface spectra similar to
353 CM2 chondrites (Cloutis et al., 2011) and are thus good family candidates for PCA 91008,
354 PCA 02012 and/or QUE 93005. New Polana and Eulalia asteroid family are thought to be at
355 the origin of Bennu asteroid (Bottke et al., 2015). Bennu has similar thermal infrared spectral
356 features as CM chondrites (Hamilton et al., 2019) and is currently being investigated by the
357 OSIRIS-REx mission. Both families are ideally placed in the inner portion of the main belt to
358 escape from the asteroid belt to Earth. While the uncertainties on the ages are large, this
359 illustrates a certain consistency between astronomical observation and meteoritic record and
360 suggest that the heating event at the origin of the thermal metamorphism of the heated CM
361 may originate in the disruptive events at the origin of the asteroid families.

362 iii) Last, many near-Earth asteroids that have been visited by spacecrafts are rubble-
363 piles, and that are explained today by catastrophic collisions (Michel et al., 2005). The rubble-
364 pile forming collision could also have played a role in setting the Rb/Sr age of the heated CM
365 chondrites. It is possible that family-forming collisions generate rubble-piles and that (ii) =
366 (iii). From a modelling perspective it appears possible (Michel et al., 2001).

367 CRE ages have already been used to link weakly heated chondrites with their asteroid
368 counterparts. Meier et al. (2016) compared CRE ages of Jbilet Winselwan (King et al., 2019)
369 with the timing of the disruption of the parent body of Veritas family. The combination of
370 several techniques may improve our understanding on the relation between meteorites and
371 asteroids families in the asteroid belt.

372

373 Conclusion

374 We developed a new model to date the heating event of aqueously altered and thermally
375 metamorphosed chondrites using Rb-Sr chronology and applied it to five heated CM
376 chondrites. The five chondrites were heated during the two last billion years excluding ^{26}Al
377 radioactive decay as the origin of the heating. These young ages more likely reflect collision
378 forming events in the asteroid belt. Our model age results are consistent with the estimated
379 ages of impacts of C-type asteroids from physical observations, suggesting that in the future
380 we may be able to link a heated chondrite with its asteroid family by comparing ages.

381

382 Acknowledgements

383 Firstly, we would like to thank the two anonymous reviewers for thorough reviews
384 that have greatly improve the quality of the paper and the editor for very efficient
385 editorial handling. FM acknowledges funding from the European Research Council
386 under the H2020 framework program/ERC grant agreement #637503 (Pristine) and
387 financial support of the UnivEarthS Labex program at Sorbonne Paris Cité (ANR-10-
388 LABX- 0023 and ANR-11-IDEX-0005-02), and the ANR through a chaire
389 d'excellence Sorbonne Paris Cité. PB acknowledges funding from the H2020
390 European Research Council (ERC) (SOLARYS ERC-CoG2017_771691).
391

392

393 References

394 Akai, J. 1988 Incompletely transformed serpentine-type phyllosilicates in the matrix of
395 antarctic cm chondrites. *Geochim. Cosmochim. Acta* 52, 1593–1599.

396 Alexander, C. M. O., Bowden, R., Fogel, M. L., & Howard, K. T. 2015 Carbonate
397 abundances and isotopic compositions in chondrites. *Meteorit. Planet. Sci.* 50, 810–833.

- 398 Alexander, C. M. O., Bowden, R., Fogel, M. L., Howard, K. T., Herd, C. D. K., & Nittler, L.
399 R. 2012 The Provenances of Asteroids, and Their Contributions to the Volatile Inventories of
400 the Terrestrial Planets. *Science* 337, 721.
- 401 Alexander, C. M. O., Howard, K. T., Bowden, R., & Fogel, M. L. 2013 The classification of
402 CM and CR chondrites using bulk H, C and N abundances and isotopic compositions.
403 *Geochim. Cosmochim. Acta* 123, 244–260.
- 404 Alexander, C. M. O., Newsome, S. D., Fogel, M. L., Nittler, L. R., Busemann, H., & Cody,
405 G. D. 2010 Deuterium enrichments in chondritic macromolecular material—implications for
406 the origin and evolution of organics, water and asteroids. *Geochim. Cosmochim. Acta* 74,
407 4417–4437.
- 408 Amsellem, E., Moynier, F., Day, J. M. D., Moreira, M., Puchtel, I. S. & Teng, F-Z. 2018 The
409 stable strontium isotopic composition of ocean island basalts, mid-ocean ridge basalts, and
410 komatiites. *Chem. Geol.* 483, 595-602.
- 411 Balcaen, L., Schrijver, I. D., Moens, L., & Vanhaecke, F. 2005 Determination of the
412 ⁸⁷Sr/⁸⁶Sr isotope ratio in usgs silicate reference materials by multi-collector ICP mass
413 spectrometry. *Inter. J. Mass Spectromet.* 242, 251–255.
- 414 Beck, P., Garenne, A., Quirico, E., Bonal, L., Montes-Hernandez, G., Moynier, F., & Schmitt,
415 B. 2014 Transmission infrared spectra (2–25 μm) of carbonaceous chondrites (CI, CM, CV–
416 CK, CR, C2 ungrouped): Mineralogy, water, and asteroidal processes. *Icarus* 229, 263–277.
- 417 Beck, P., Gillet, P., El Goresy, A., & Mostefaoui, S. 2005 Timescales of shock processes in
418 chondritic and martian meteorites. *Nature* 435, 1071–1074.
- 419 Bottke, W. F., Vokrouhlicky, D., Walsh, K. J., Delbo, M., Michel, P., Lauretta, D. S.,
420 Campins, H., Connolly Jr., H. C., Scheeres, D. J. & Chelsey, S. R. 2015 In search of the
421 source of asteroid (101955) Bennu: Applications of the stochastic YORP model. *Icarus* 247,
422 191-217.
- 423 Brož, M., Morbidelli, A., Bottke, W. F., Rozehnal, J., Vokrouhlicky, D. & Nesvorný, D. 2013
424 Constraining the cometary flux through the asteroid belt during the late heavy bombardment.
425 *A&A* 551, A117.
- 426 Carruba, V., Domingos, R. C., Nesvorný, D., Roig, F., Huaman, M. E., & Souami, D. 2013 A
427 multidomain approach to asteroid families' identification. *MNRAS* 433, 2075–2096.
- 428 Chapman, C. R., Morrison, D., & Zellner, B. 1975 Surface properties of asteroids: A
429 synthesis of polarimetry, radiometry, and spectrophotometry. *Icarus* 25, 104–130.

- 430 Clayton, R. N. & Mayeda, T. K. 1999 Oxygen isotope studies of carbonaceous chondrites.
431 *Geochim. Cosmochim. Acta* 63, 2089–2104.
- 432 Cloutis, E. A., Hudon, P., Hiroi, T., Gaffey, M. J., & Mann, P. 2011 Spectral reflectance
433 properties of carbonaceous chondrites: 2. CM chondrites. *Icarus* 216, 309– 346.
- 434 Connelly, J.N. Bizzarro, M., Krot, A. N., Nordlund, A., Wielandt, D., Ivanova, M. A. 2012
435 The absolute chronology and thermal processing of solids in the solar protoplanetary disk.
436 *Science* **338**, 651–655. SEP
- 437 Eugster, O., F. Herzog, G., Marti, K., & Caffee, M. 2006 Irradiation records, cosmic-ray
438 exposure ages, and transfer times of meteorites. *Meteorit. Early Solar System II*.
- 439 Farinella, P. & Davis, D. R. 1992 Collision rates and impact velocities in the main asteroid
440 belt. *Icarus* 97, 111–123.
- 441 Garenne, A., Beck, P., Montes-Hernandez, G., Chiriac, R., Toche, F., Qui- rico, E., Bonal, L.,
442 & Schmitt, B. 2014 The abundance and stability of water in type 1 and 2 carbonaceous
443 chondrites (CI, CM and CR). *Geochem. Cosmochim. Acta* 137, 93–112.
- 444 Hamilton, V. E. et al. 2019 Evidence for widespread hydrated minerals on asteroid (101955)
445 Bennu. *Nat. Astro.* 3, 332-340.
- 446 Hans, U., Kleine, T., & Bourdon, B. 2013 Rb–sr chronology of volatile depletion in
447 differentiated protoplanets: Babi, ador and all revisited. *Earth Planet. Sci. Lett.* 374, 204–214.
- 448 Hiroi, T., Pieters, C. M., Zolensky, M. E., & Lipschutz, M. E. 1993 Evidence of thermal
449 metamorphism on the C, G, B, and F asteroids. *Science* 261, 1016–8.
- 450 Jenniskens, P., Fries, M. D., Yin, Q.-Z., Zolensky, M., Krot, A. N., Sandford, S. A., Sears, D.,
451 et al. 2012 Radar-enabled recovery of the Sutter’s Mill meteorite, a carbonaceous chondrite
452 regolith breccia. *Science* 338, 1583.
- 453 Johnson, T. V. & Fanale, F. P. 1973 Optical properties of carbonaceous chondrites and their
454 relationship to asteroids. *J. Geophys. Res.* 78, 8507–8518.
- 455 Kaushal, S. K. & Wetherill, G. W. 1970 Rubidium 87–strontium 87 age of carbonaceous
456 chondrites. *J. Geophys. Res.* 75, 463–468.
- 457 King, A. J., Russel, S. S., Schofield, P. F., Humphreys-Williams, E. R., Strekopytov, S.,
458 Abernethy, F. A. J., Verchovsky, A. B. & Grady, M. M. 2019 The alteration history of the
459 Jbilet Winselwan CM carbonaceous chondrite: An analog for C-type asteroid sample return.

- 460 Meteorit. Planet. Sci. 54 521-543.
- 461 Kitazato, K. et al. 2019 The surface composition of asteroid 162173 Rygu from Hayabusa2
462 near-infrared spectroscopy. *Science*, 364 272-275.
- 463 Lee, T., Papanastassiou, D. A. & Wasserburg, G. J. 1977 Aluminium-26 in the early solar
464 system - Fossil or fuel. *Astrophys. J.* 211, 107-110.
- 465 Lindgren, P., Hanna, R. D., Dobson, K. J., Tomkinson, T. & Lee, M. R. 2015 The paradox
466 between low shock-stage an evidence for compaction in CM carbonaceous chondrites
467 explained by multiple low-intensity impacts. *Geochim. Cosmochim. Acta* 148, 159-178.
- 468 Lodders, K. 2003 Solar system abundances and condensation temperatures of the elements.
469 *Astrophys. J.* 591, 1220–1247.
- 470 Mahan, B., Moynier, F., Beck, P., Pringle, E. A., & Siebert, J. 2018 A history of violence:
471 Insights into post-accretionary heating in carbonaceous chondrites from volatile element
472 abundances, Zn isotopes and water contents. *Geochim. Cosmochim. Acta* 220, 19–35.
- 473 Marchi, S., Delbo, M., Morbidelli, A., Paolicchi, P., & Lazzarin, M. 2009 Heating of near-
474 Earth objects and meteoroids due to close approaches to the Sun. *Mon. Not. R. Astron. Soc.*
475 400, 147-153.
- 476 Meier, M. M. M., Grimm, S., Maden, C., Busemann, H. 2016 Do we have meteorites from the
477 Veritas asteroid break-up event 8 Ma ago? *Ann. Meteorit. Soci. Meet.* 79.
- 478 Michel, P., Benz, W., Tanga, P., & Richardson, D. C. 2001 Collisions and gravitational
479 reaccumulation: Forming asteroid families and satellites. *Science* 294, 1696.
- 480 Michel, P. & Yoshikawa, M. 2005 Earth impact probability of the asteroid (25143) Itokawa to
481 be sampled by the spacecraft Hayabusa. *Icarus* 179, 291–296.
- 482 Milani, A., Cellino, A., Knežević, Z., Novaković, B., Spoto, F., & Paolicchi, P. 2014 Asteroid
483 families classification: Exploiting very large datasets. *Icarus* 239, 46–73.
- 484 Milani, A., Knežević, Z., Spoto, F., Cellino, A., Novaković, B., & Tsirvoulis, G. 2017 On the
485 ages of resonant, eroded and fossil asteroid families. *Icarus* 288, 240–264.
- 486 Mittlefehldt, D. W. & Wetherill, G. W. 1979 Rb-Sr studies of CI and CM chondrites.
487 *Geochim. Cosmochim. Acta* 43, 201–206.
- 488 Morbidelli, A. & Gladman, B. 1998 Orbital and temporal distributions of meteorites
489 originating in the asteroid belt. *Meteorit. Planet. Sci.* 33, 999–1016.

490 Moynier, F., Day, J., Wataru, O., Yokoyama, T., Bouvier, A., J. Walker, R., & A. Podosek, F.
491 2012 Planetary-scale strontium isotopic heterogeneity and the age of volatile depletion of
492 early solar system materials. *Astrophys. J.* 758, 45–51.

493 Nakamura, T. 2005 Post-hydration thermal metamorphism of carbonaceous chondrites. *J.*
494 *Miner. Petrol. Sci.* 100, 260–272.

495 Nakamura, T., Okazaki, R., & Huss, G. R. 2006 Thermal metamorphism of CM carbonaceous
496 chondrites: effects on phyllosilicate mineralogy and presolar grain abundances. *Lunar Planet.*
497 *Sci.* 37.

498 Nakato, A., Brearley, A. J., Nakamura, T., Noguchi, T., Ahn, I., Lee, J. I., Matsuoka, M., &
499 Sasaki, S. 2013 PCA 02012: A unique thermally metamorphosed carbonaceous chondrite.
500 *Lunar Planet. Sci.* 44.

501 Nakato, A., Nakamura, T., Kitajima, F., & Noguchi, T. 2008 Evaluation of dehydration
502 mechanism during heating of hydrous asteroids based on mineralogical and chemical analysis
503 of naturally and experimentally heated cm chondrites. *Earth, Planet. Space* 60, 855–864.

504 Nebel, O., Mezger, K., & van Westrenen, W. 2011 Rubidium isotopes in primitive chondrites:
505 Constraints on Earth's volatile element depletion and lead isotope evolution. *Earth Planet.*
506 *Sci. Lett.* 305, 309–316.

507 Paolicchi, P., Spoto, F., Knežević, Z., & Milani, A. 2018 Ages of asteroid families estimated
508 using the YORP-eye method. *MNRAS* 484, 1815–1828.

509 Papanastassiou, D. A. & Wasserburg, G. J. 1969 Initial strontium isotopic abundances and the
510 resolution of small time differences in the formation of planetary objects. *Earth Planet. Sci.*
511 *Lett.* 5, 361–376.

512 Pringle, E. A. & Moynier, F. 2017 Rubidium isotopic composition of the earth, meteorites,
513 and the moon: Evidence for the origin of volatile loss during planetary accretion. *Earth*
514 *Planet. Sci. Lett.* 473, 62–70.

515 Quirico, E., Bonal, L., Beck, P., Alexander, C., Yabuta, H., Nakamura, T., Nakato, A.,
516 Flandinet, L., Montagnac, G., Schmitt-Kopplin, P., & Herd, C. D. K. 2018 Prevalence and
517 nature of heating processes in CM and C2-ungrouped chondrites as revealed by insoluble
518 organic matter. *Geochim. Cosmochim. Acta* 241.

519 Quirico, E., Garenne, A., Beck, P., Flandinet, L., Bonal, L., & Montagnac, G. 2013
520 Collisions-induced thermal metamorphism in CM chondrites as revealed by organic matter.
521 *Ann. Meteorit. Soci. Meet.* 76.

- 522 Quirico, E., Orthous Daunau, F.-R., Beck, P., Bonal, L., Briani, G., Bourot- Denise, M.,
523 Montagnac, G., Dobrica, E., Engrand, C., Charon, E., Rouzard, J.-N., & Gounelle, M. 2011
524 Pre-accretion heterogeneity of organic matter in types 1 and 2 chondrites. *Lunar Planet. Sci.*
525 42.
- 526 Rubin, A. E. 1995 Petrologic evidence for collisional heating of chondritic asteroids. *Icarus*
527 113, 156–167.
- 528 Rubin, A. E. 2012 Collisional facilitation of aqueous alteration of CM and CV carbonaceous
529 chondrites. *Geochim. Cosmochim. Acta* 90, 181–194.
- 530 Rubin, A. E., Trigo-Rodríguez, J. M., Huber, H., & Wasson, J. T. 2007 Progressive aqueous
531 alteration of CM carbonaceous chondrites. *Geochim. Cosmochim. Acta* 71, 2361–2382.
- 532 Schmitt, R. T., Deutsch, A., & Stoffler, D. 1994 Calculation of Hugoniot curves and post-
533 shock temperatures for H and L chondrites. *Lunar Planet. Sci.* 25.
- 534 Schudel, G., Lai, V., Gordon, K., & Weis, D. 2015 Trace element characterization of USGS
535 reference materials by HR-ICP-MS and Q-ICP-MS. *Chem. Geol.* 410, 223–236.
- 536 Spoto, F., Milani, A., & Knežević, Z. 2015 Asteroid family ages. *Icarus* 257, 275– 289.
- 537 Sugita, S. et al. 2019 The geomorphology, color, and thermal properties of Ryugu:
538 Implications for parent-body processes. *Science* 364, Issue 6473.
- 539 Tomeoka, K., Kiriyama, K., Nakamura, K., Yamahana, Y., & Sekine, T. 2003 Interplanetary
540 dust from the explosive dispersal of hydrated asteroids by impacts. *Nature* 423, 60–62.
- 541 Tonui, E. K., Zolensky, M. E., Hiroi, T., Wang, M.-S., & Lipschutz, M. E. 2002 Petrographic,
542 chemical and spectroscopic data on thermally metamorphosed carbonaceous chondrites.
543 *Lunar Planet. Sci.* 33.
- 544 Tonui, E., Zolensky, M., Hiroi, T., Nakamura, T., Lipschutz, M. E., Wang, M.-S. & Okudaira,
545 K. 2014 Petrographic, chemical and spectroscopic evidence for thermal metamorphism in
546 carbonaceous chondrites I: CI and CM chondrites. *Geochim. Cosmochim. Acta* 126, 284–306.
- 547 Tyburczy, J. A., Frisch, B., & Ahrens, T. J. 1986 Shock-induced volatile loss from a
548 carbonaceous chondrite: implications for planetary accretion. *Earth Planet. Sci. Lett.* 80, 201–
549 207.
- 550 Vernazza, P., Binzel, R. P., Thomas, C. A., DeMeo, F. E., Bus, S. J., Rivkin, A. S., &
551 Tokunaga, A. T. 2008 Compositional differences between meteorites and near-earth asteroids.

552 Nature 454, 858.

553 Vernazza, P., Marsset, M., Beck, P., Binzel, R. P., Birlan, M., Brunetto, R., Demeo, F. E.,
554 Djouadi, Z., Dumas, C., Merouane, S., Mousis, O., & Zanda, B. 2015 Interplanetary dust
555 particles as samples of icy asteroids. *Astrophys. J.* 806.

556 Vernazza, P., Zanda, B., Binzel, R. P., Hiroi, T., DeMeo, F. E., Birlan, M., Hewins, R., Ricci,
557 L., Barge, P., & Lockhart, M. 2014 Multiple and fast: the accretion of ordinary chondrite
558 parent bodies. *Astrophys. J.* 791.

559 Walsh, K. J. , Delbó, M., Bottke, W. F., Vokrouhlicky, D. & Lauretta, D. S. 2013 Introducing
560 the Eulalia and new Polana asteroid families: re-assessing primitive asteroid families in the
561 inner Main Belt. *Icarus* 225, 283-297.

562 Wang, M.-S. & Lipschutz, M. E. 1998 Thermally metamorphosed carbonaceous chondrites
563 from data for thermally mobile trace elements. *Meteorit. Planet. Sci.* 33, 1297–1302.

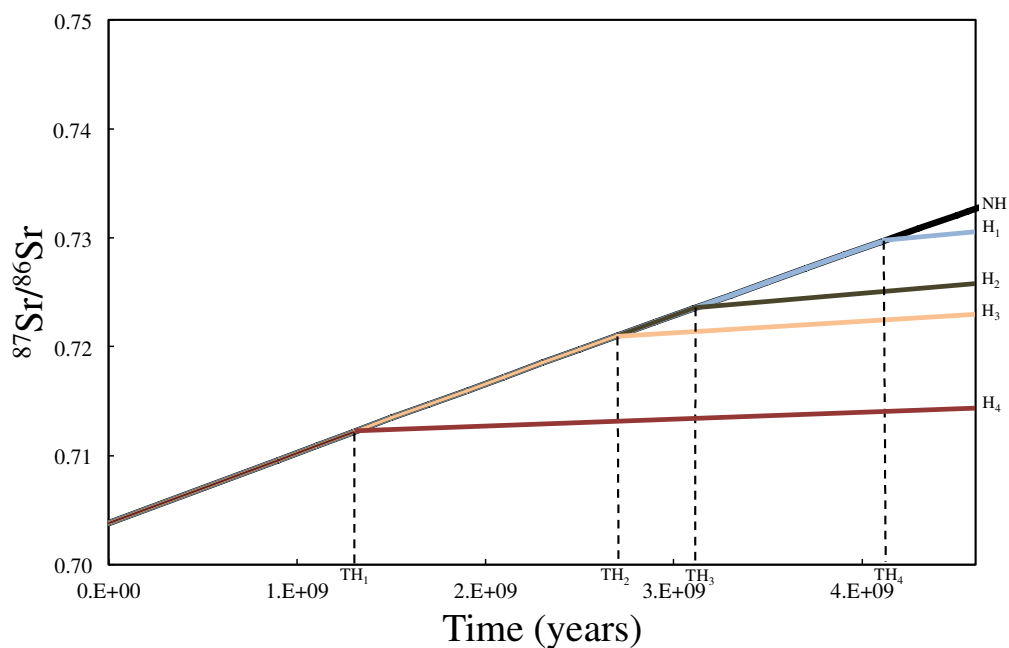
564 Wasson, J. T., Rubin, A. E., & Benz, W. 1987 Heating of primitive, asteroid-size bodies by
565 large impacts. *Meteoritics* 22.

566

567

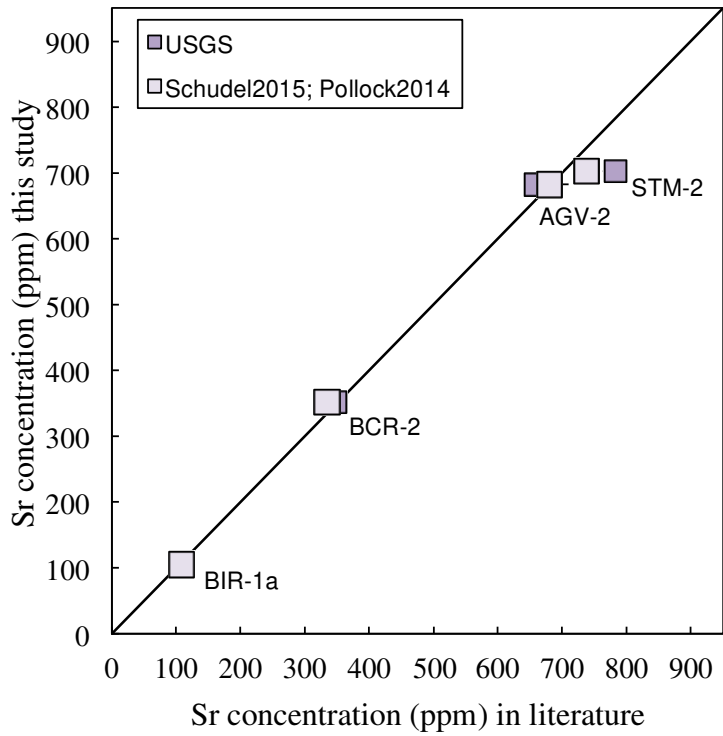
568 Figures

569 Figure 1



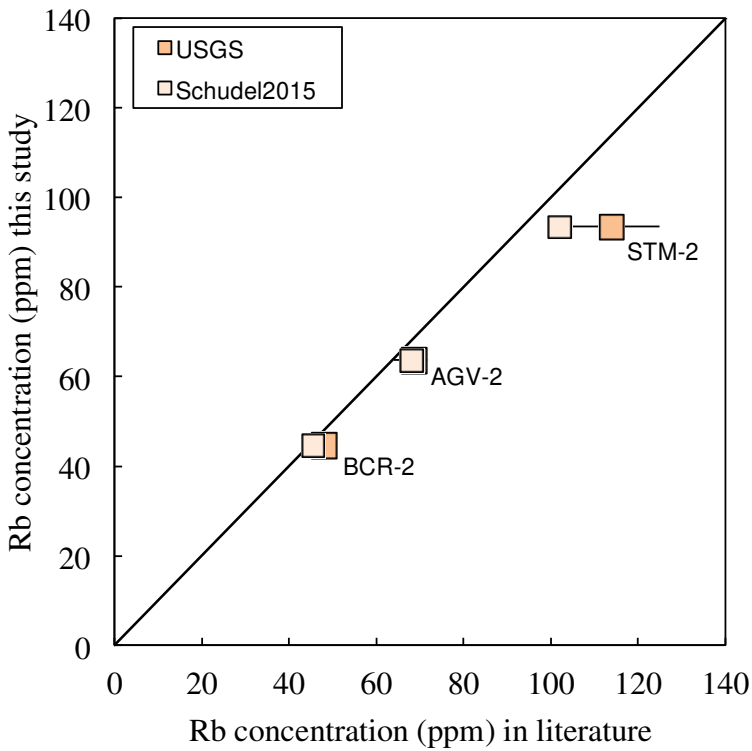
570

571 Figure 2a



572

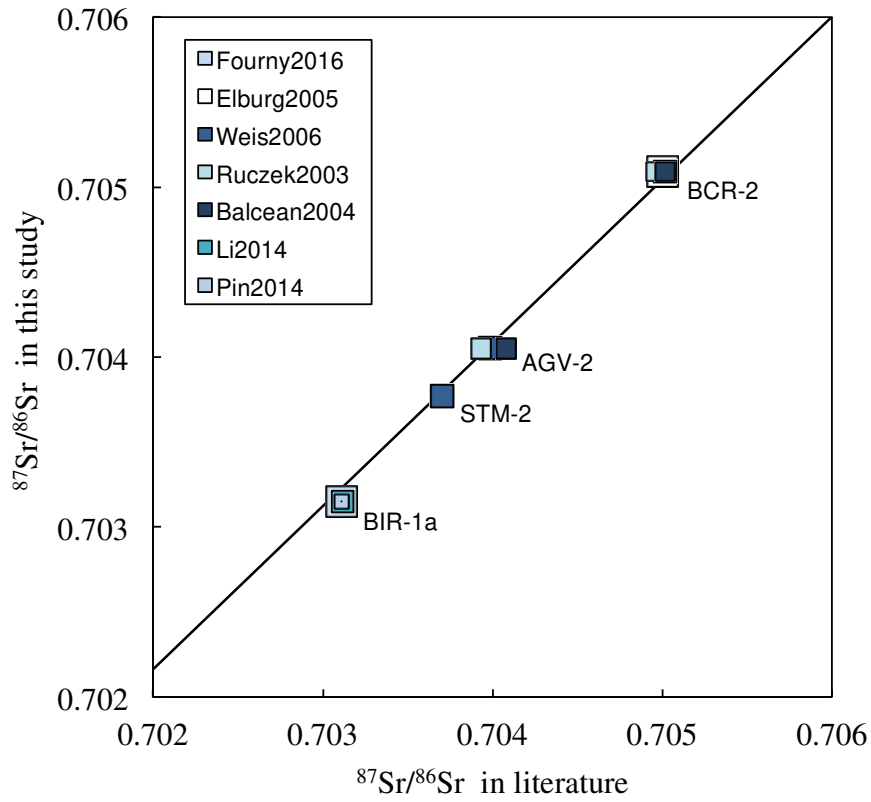
573 Figure 2b



574

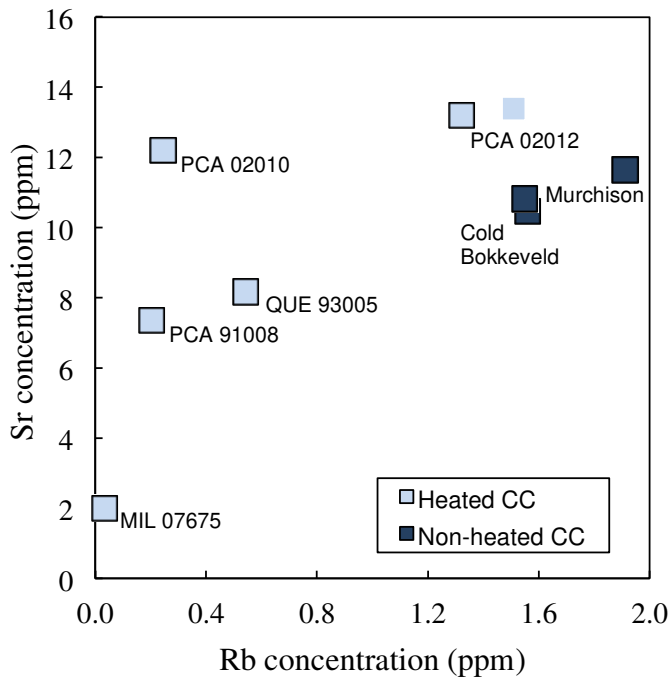
575 Figure 2c

576

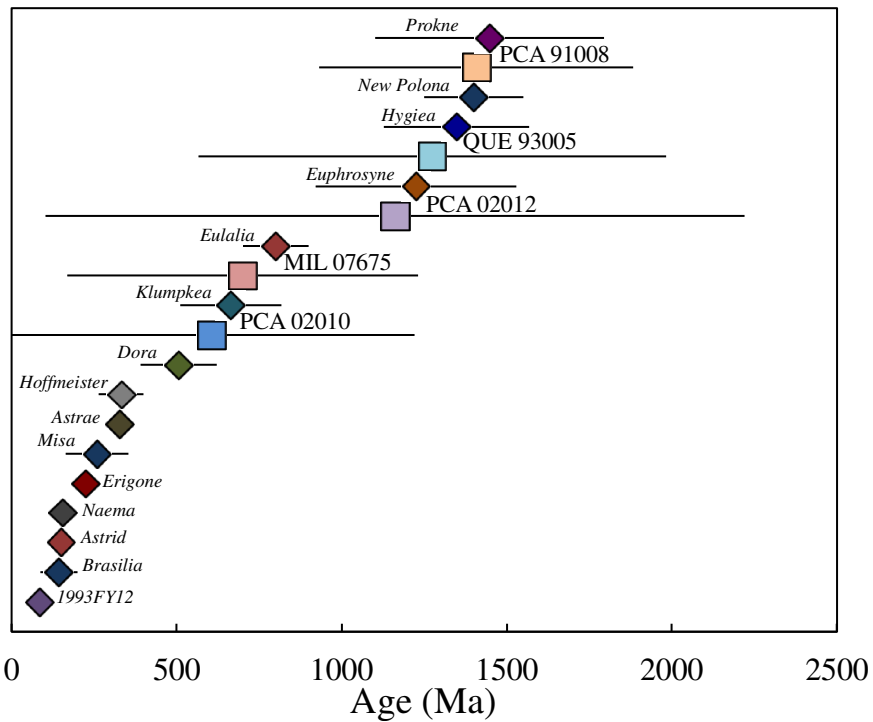


577

578 Figure 3



579



580 Figure 4

581

582 Captions

583

584 Figure 1: Fictive Evolution of the $^{87}\text{Sr}/^{86}\text{Sr}$ ratio of bulk chondrites (H_x) that occurred heating
 585 event at different time (TH_x) showing the use of Rb/Sr radiochronology to estimate the date of
 586 the heating event.

587

588 Figure 2: Sr (a) and Rb (b) concentrations and $^{87}\text{Sr}/^{86}\text{Sr}$ (c) ratios of terrestrials standards
 589 conducted in this study compare to the literature. The black line represents 1:1 slope.

590

591 Figure 3: Sr concentration of heated and non-heated CM chondrites relative to their Rb
 592 content. The light blue square symbol without an outline is the replicate of PCA 02012.

593

594 Figure 4: Estimation of the ages of heated CM (square symbols) compared to ages of
 595 collisional C-type asteroids family (diamond symbols) from Paolicchi et al. (2018).

596

Table 1

Rb and Sr concentration, $^{87}\text{Sr}/^{86}\text{Sr}$ and $^{87}\text{Rb}/^{86}\text{Sr}$ ratios of terrestrial basalts and heated CM chondrites

Sample	$^{87}\text{Sr}/^{86}\text{Sr}$	$2se^1$	[Sr] ppm	error ²	[Rb] ppm	error ²	$^{87}\text{Rb}/^{86}\text{Sr}$	error ²
Heated CM chondrites								
PCA 02010	0.73010	0.00014	12.21	0.08	0.245	0.0027	0.057	0.001

PCA02012 #1	0.72984	0.00009	13.21	0.10	1.320	0.0062	0.289	0.003
PCA02012 #1	0.72968	0.00003	13.39	0.09	1.509	0.0152	0.326	0.004
<i>Average</i>	0.72976	0.00022	13.30	0.26	1.415	0.27	0.308	0.052
PCA 91008	0.72438	0.00009	7.36	0.05	0.205	0.0013	0.079	0.001
QUE 93005	0.72801	0.00002	8.17	0.06	0.542	0.0023	0.191	0.002
MIL 07675	0.72898	0.00006	2.00	0.03	0.033	0.0004	0.043	0.001
Terrestrial basalts								
BIR-1a	0.70315	0.00004	105.50	0.24	-	-	-	-
AGV-2	0.70405	0.00004	682.79	0.56	63.67	0.41	0.270	0.019
STM-2	0.70377	0.00004	701.66	0.52	93.47	0.49	0.385	0.027
BCR-2	0.70509	0.00006	352.20	0.45	44.58	0.05	0.366	0.025

¹ 2se= 2 x standard deviation / \sqrt{n}

² the error is estimated using a propagation law of error

Table 2

Age estimation of the heating event of five heated chondrites in Ma

	Minimum value <i>Murchison</i>	Maximum value <i>Mighei</i>	Mean value	Standard error	Heating Stage
PCA 02010	-7	1221	607	614	
PCA02012 #1	102	2220	1161	1059	III/IV
PCA02012 #2	254	2580	1417	1163	
PCA 91008	1068	2019	1544	475	III

QUE 93005	566	1982	1274	708	I/II
------------------	-----	------	-------------	------------	------

MIL 07675	168	1231	699	531	-
------------------	-----	------	------------	------------	---

597